Geophysical Prospecting EAGE EUROPEAN ASSOCIATION OF GEOSCIENTISTS & ENGINEERS

Geophysical Prospecting doi: 10.1111/j.1365-2478.2010.00866.x

Migration for velocity and attenuation perturbations

Bobby Hak[1]* and Wim A. Mulder[1,2]

[1]*Delft University of Technology, Department of Geotechnology, Stevinweg 1, 2628 CN Delft, the Netherlands, and* [2]*Shell International Exploration and Production B.V., Kessler Park 1, 2288 GS Rijswijk, the Netherlands*

Received March 2009, revision accepted November 2009

ABSTRACT

Migration maps seismic data to reflectors in the Earth. Reflections are not only caused by small-scale variations of the velocity and density but also of the quality factor that describes attenuation. We investigated scattering due to velocity and attenuation perturbations by computing the resolution function or point-spread function in a homogeneous background model. The resolution function is the migration image of seismic reflection data generated by a point scatterer. We found that the resolution function mixes velocity and attenuation parameter perturbations to the extent that they cannot be reconstructed independently. This is true for a typical seismic setting with sources and receivers at the surface and a buried scatterer. As a result, it will be impossible to simultaneously invert for velocity and attenuation perturbations in the scattering approach, also known as the Born approximation.

We proceeded to investigate other acquisition geometries that may resolve the ambiguity between velocity and attenuation perturbations. With sources and receivers on a circle around the scatterer, in 2D, the ambiguity disappears. It still shows up in a cross-well setting, although the mixing of velocity and attenuation parameters is less severe than in the surface-to-surface case. We also consider illumination of the target by diving waves in a background model that has velocity increasing linearly with depth. The improvement in illumination is, however, still insufficient to remove the ambiguity.

Key words: Attenuation, Migration, Acquisition.

1 INTRODUCTION

Migration maps seismic data recorded at the Earth's surface into an image of the subsurface. Although qualitative structural images are often acceptable, quantitative characterization of a scatterer's reflection and attenuation properties may enable a distinction between fluid-bearing and gas- or air-filled geological formations. For migration, the implicit assumption is that the data only contain primaries and that surface or interbed multiples are absent or negligible. We can generate such data with the linearized wave equation or Born approximation. In this approximation, the subsurface model is split into a part that does not produce reflections and a perturbation that generates the reflection data. One way to obtain a background model that does not generate reflections in the seismic frequency band is the choice of a smooth model. The differences between the original model that may contain hard contrasts in material properties and its smooth version can be viewed as perturbations. Migration of seismic data then provides a reconstruction of these reflectors. In this setting, impedance contrasts become velocity and density perturbations. They are not the only perturbations that create reflections. Attenuation perturbations can do that as well (e.g., Vasheghani and Lines 2009). The formulation of the migration operator in the frequency domain naturally lends itself for imaging of velocity, density, and attenuation perturbations in a given smooth background model. The goal of this paper

---

*E-mail: b.hak@tudelft.nl

is to study migration in this context. For simplicity, we consider the constant-density acoustic wave equation. Impedance perturbations are thereby reduced to velocity perturbations.

From a mathematical point of view, migration can be viewed as the gradient or sensitivity of the least-squares error functional with respect to the model parameters (Lailly 1983; Tarantola 1984). The error functional is the sum of squared differences between modelled and observed data. A gradient-based optimization algorithm can attempt to find the model that best explains the data. Because seismic data are band-limited, this minimization problem is plagued by spurious local minima, making full waveform inversion difficult except when a very good initial model is available, so that gradient-based optimization will end up in a nearest minimum that is actually the global minimum, or when waveform tomography can be performed, in a cross-well setting or with diving waves from the surface of the Earth. See, for example, papers by Tarantola (1984, 1986), Mora (1987, 1988, 1989), Crase *et al.* (1990, 1992), Pratt (1999), Hicks and Pratt (2001), Shin, Jang and Min (2001), Shipp and Singh (2002), Operto *et al.* (2004), Barnes, Charara and Tsuchiya (2008), Royle and Singh (2008), and many others. The least-squares problem can be simplified by linearization of the inverse problem. This is equivalent to using the Born approximation for the forward modelling problem. The model parameters then become, for instance, the impedance perturbations of the background model. Minimization of the least-squares functional still makes sense in this context. The data should then be restricted to primaries. The result of the minimization will be a band-limited reconstruction of the reflectivity, deconvolved for the source wavelet (Jin *et al.* 1992; Lambaré *et al.* 1992; Nemeth, Wu and Schuster 1999; Østmo, Mulder and Plessix 2002; Mulder and Plessix 2004; Plessix and Mulder 2004; Gélis, Virieux and Grandjean 2007). Algorithmically, this approach resembles full waveform inversion. However, as the inverse problem is now linear in the model parameters, a preconditioned conjugate-gradient method suffices to find the best reflectivity model.

Application of the conjugate-gradient method has the advantage that the convergence of the method will not be affected by the presence of null-space components. A suitable preconditioner will accelerate convergence to the model that best explains the data. If there are null-space components, the conjugate-gradient method without a preconditioner will converge to the minimum-norm solution. With a preconditioner, the method will converge to a different solution that has the smallest weighted norm. The preconditioner implicitly defines the weighting. The inverse of the Hessian, the second derivative of the least-squares cost functional with respect to the model parameters, is the best preconditioner but is computationally out of reach for large-scale problems. In spite of this, it was considered by Pratt, Shin and Hicks (1998). In this paper, we will compute and use it to better understand attenuation imaging.

Estimating attenuation is usually restricted to the background model. Causse, Mittet and Ursin (1999), Hicks and Pratt (2001), and Innanen and Weglein (2007) presented examples for nonlinear inversion. Incorporation of attenuation in the reflectivity was considered by Ribodetti, Virieux and Durand (1995) and Ribodetti and Virieux (1998). The goal of the present paper is to obtain insight into the problems that surround the imaging of attenuation perturbations. A method for the estimation of multiple parameters was presented by Kennett, Sambridge and Williamson (1988) and Kennett and Sambridge (1998), but this approach will not be considered here. Mulder and Hak (2009) showed that simultaneous imaging of velocity and attenuation perturbation with the Born approximation of the constant-density visco-acoustic wave equation leads to an ambiguity: the data can be equally well explained by a velocity perturbation or by an attenuation perturbation. There exists a simple transformation between these two models for 1D, horizontally layered scattering models in a constant background. Here, we elaborate on the subject by considering several acquisition geometries with the purpose of finding one that alleviates or removes the ambiguity. We consider simple 2D examples for which the Green functions are available and the full Hessian can be readily computed. In earlier publications (Hak and Mulder 2008a,b), we considered various non-diagonal preconditioners for the linearized inverse problems but once we realized the existence of the ambiguity mentioned above, we concluded that such preconditioning will never help in providing a proper answer.

The goal of our paper is to study the occurrence of the ambiguity between velocity and attenuation perturbations for two simple background models and investigate if there exist acquisition geometries that provide sufficient illumination to reduce its effect or even completely remove it. We will stick to the Born approximation, despite its limited validity, because of its natural correspondence to seismic migration. In Section 2, we formulate the problem of estimation velocity and attenuation parameters. Section 3 describes the migration of surface data for a buried point scatterer in a homogeneous background model and the result of its reconstruction based on the pseudo-inverse of the Hessian. We proceed in Section 4 with a circular and a cross-well acquisition in order to investigate if this will remove the ambiguity. Also, a velocity model that increases linearly with depth is considered, because it will lead to diving waves that improve the illumination of the target as long as it is not located too deeply (Mulder and Plessix 2008). Finally, we summarize and discuss the results.

2 PROBLEM STATEMENT

The constant-density visco-acoustic wave equation in the frequency domain reads

$$-\omega^2 \tilde{m}\,\tilde{p} - \Delta \tilde{p} = S,$$

with pressure $\tilde{p}(\omega, \mathbf{x})$ depending on position $\mathbf{x}$ and angular frequency $\omega = 2\pi f$ at frequency f, source term $S(\omega, \mathbf{x})$, and model parameters (Aki and Richards 1980)

$$\tilde{m}(\mathbf{x}) = \frac{1}{v^2} = \frac{1}{c^2}\left[1 - \frac{2}{\pi Q}\log(f/f_r) + \frac{\mathrm{i}}{Q}\right]. \tag{1}$$

The sound speed is $c(\mathbf{x})$. The quality factor $Q(\mathbf{x})$ describes attenuation. The logarithmic term is required for causality and is defined relative to some reference frequency f_r. Because we are interested in imaging reflectors or scatterers, we use the Born approximation. Let $\tilde{m} = m_b + m$, where $m_b(\mathbf{x})$ represents a smooth background velocity model that does not produce significant reflections in the seismic frequency band. The Born approximation is represented by the pair of equations

$$-\omega^2 m_b\, p_b - \Delta p_b = S, \tag{2}$$

$$-\omega^2 m_b\, p\ - \Delta p\ = \omega^2 m\, p_b. \tag{3}$$

The background pressure wavefield is denoted by p_b and the reflection data by p. For simplicity, we will assume that m is independent of ω, so the frequency-dependent correction term is ignored in the scattering model but not in the background model. Hence, a perturbation of the real part of m relates to a velocity perturbation, $\delta(c^{-2}) = c^{-2} - c_b^{-2}$, whereas a perturbation of the imaginary part of m relates to a perturbation of a combination of the velocity and the quality factor, $\delta(c^{-2}Q^{-1}) = c^{-2}Q^{-1} - c_b^{-2}Q_b^{-1}$. Note that for a purely imaginary perturbation, $\delta(c^{-2}) = 0$ and $\delta(c^{-2}Q^{-1}) = c_b^{-2}(Q^{-1} - Q_b^{-1})$, meaning that we only have a perturbation in the quality factor that describes the attenuation.

For a delta-function source at position $\mathbf{x}_s$ with wavelet $w(\omega), S = w(\omega)\delta(\mathbf{x} - \mathbf{x}_s)$, the solution at some receiver location $\mathbf{x}_r$ can be expressed by equation (3.2.1) of Bleistein, Cohen and Stockwell (2000), which in our notation becomes

$$p_{r(s)} = p(\omega, \mathbf{x}_r) = w(\omega)\int d\mathbf{x}\, \omega^2 G(\omega, \mathbf{x}_s, \mathbf{x}) m(\mathbf{x}) G(\omega, \mathbf{x}, \mathbf{x}_r). \tag{4}$$

The Green function $G(\omega, \mathbf{x}_1, \mathbf{x}_2)$ is determined by the background model $m_b(\mathbf{x})$ and describes the wavefield at position $\mathbf{x}_2$ when equations (2) and (3) are solved for a delta-function source at $\mathbf{x}_1$ with unit wavelet in the frequency domain. Equation (4) represents a linear map from $m(\mathbf{x})$ to $p_{r(s)}$, which we represent as $\mathbf{p} = \mathsf{F}\mathbf{m}$. Here $\mathbf{p}$ is the seismic data set with primary reflections only, for all shots, labelled by s, receivers $r(s)$, and frequencies ω. Note that F depends on the background model m_b, the acquisition, and the source wavelet.

Migration maps the data back to the subsurface according to $\mathbf{g} = \mathsf{F}^{\mathsf{H}}\mathbf{p}$. The superscript $(\cdot)^{\mathsf{H}}$ denotes the complex conjugate transpose. For a given model $\mathbf{m}$, this implies that the migration image can be expressed as $\mathbf{g} = \mathsf{H}\mathbf{m}$, with $\mathsf{H} = \sum_\omega \mathsf{F}^{\mathsf{H}}\mathsf{F}$. The operator H describes how a given reflectivity model is transformed into an image after forward modelling and migration, given a certain acquisition. If $m(\mathbf{x}) = \delta(\mathbf{x} - \mathbf{x}_p)$ is a delta-function or spike in a single position $\mathbf{x}_p$, then $\mathsf{H}\,\delta(\mathbf{x} - \mathbf{x}_p)$ describes how closely the corresponding migration image matches its original. Several authors have therefore referred to $\mathsf{H}\,\delta(\mathbf{x} - \mathbf{x}_p)$ as the point-spread function (Devaney 1984; Gjøystdal *et al.* 2002) or resolution function (von Seggern 1991; Wapenaar 1997; Chen and Schuster 1999; Berkhout *et al.* 2001; Toxopeus *et al.* 2004, 2008). Lailly (1983) and Tarantola (1984) showed that the gradient or sensitivity of the least-squares error functional is a migration image. If $p^{\mathrm{obs}}_{r(s)}(\omega)$ denotes the observed data and $p_{r(s)}(\omega)$ the synthetic data for some model $m(\mathbf{x})$, the least-squares functional is

$$\mathcal{J} = \frac{1}{2}\sum_{\omega}\sum_{s}\sum_{r(s)}\left|p_{r(s)}(\omega) - p^{\mathrm{obs}}_{r(s)}(\omega)\right|^2.$$

The gradient or sensitivity of $\mathcal{J}$ with respect to the model parameters is denoted by $\mathbf{g}$. Its elements $g(\mathbf{x})$ are the derivatives of $\mathcal{J}$ with respect to the real and imaginary part of $m(\mathbf{x})$ in the points $\mathbf{x}$.

Minimization of the cost functional $\mathcal{J}$ subject to equations (2) and (3) can be accomplished with a gradient-based descent method, for instance, the conjugate-gradient method (Østmo *et al.* 2002). The conjugate-gradient method has the useful property of finding a minimum-norm solution if the problem has a non-empty null space. Convergence can be accelerated by using the second derivatives or Hessian of the functional with respect to the model parameters. In general, the size of the Hessian makes its computation too costly, although it can be computed for small problems (Pratt *et al.* 1998; Chavent and Plessix 1999; van Houten *et al.* 1999; Plessix and Mulder 2004). It is usually more efficient to replace the Hessian by an approximation of its diagonal and use the inverse of the resulting diagonal matrix as a preconditioner for the conjugate-gradient method. This is motivated by the fact that the dominant term in the Hessian is diagonal in the asymptotic limit for high frequencies (Beylkin and Burridge 1990; ten Kroode, Smit and Verdel 1998) in the absence of multiples. The elements of the inverse of the diagonal approximation are sometimes called 'true-amplitude' migration weights. With such weights, just a single step of a preconditioned conjugate-gradient algorithm may already provide a result that is acceptable for further interpretation (Docherty 1991; Gray 1997; Chavent and Plessix 1999; Mulder and Plessix 2004; Plessix and Mulder 2004). An alternative was presented by Rickett (2003) and Guitton (2004), based on migration, demigration and remigration, followed by amplitude comparison. Symes (2008) described further improvements. In this paper, we will actually compute the full Hessian and its pseudo-inverse. For given data, this will directly provide the model at which the least-squares cost functional has its minimum.

3 RESOLUTION FUNCTION FOR A CONSTANT MODEL

As a first example, we considered the point-spread or resolution function for a point scatterer in a 2D model with a constant velocity of $c_b = 2$ km/s and quality factor $Q_b = 100$. We included the causal correction term in equation (1) with $f_r = 1$ Hz but ignored it in the reconstruction of the scatterer, so $m(\mathbf{x})$ in equation (3) is assumed to be independent of frequency. The point scatterer, $m(\mathbf{x}) = \delta(\mathbf{x} - \mathbf{x}_p)$, had a real-valued, unit amplitude and was placed at $x_p = 0$ m and $z_p = 750$ m. Receivers were positioned at zero depth from $x = -1900$ to 1900 m at a 25 m interval. Shots are located between $x = -1887.5$ and 1887.5 m at the same interval. The Green function $G(\omega, \mathbf{x}_1, \mathbf{x}_2) = \frac{i}{4} H_0^{(1)}(kr)$ with $r = [(x_2 - x_1)^2 + (z_2 - z_1)^2]^{1/2}$. The Hankel function or Bessel function of the third kind $H_0^{(1)}(x) = J_0(x) + \mathrm{i}\, Y_0(x)$ are related to the Bessel functions $J_0(x)$ of the first kind and $Y_0(x)$ of the second kind. We included a Ricker wavelet with a peak frequency of 15 Hz and used frequencies from 0.5–41 Hz with an interval of 0.5 Hz. The resulting resolution function is similar to examples by, for instance, Wu and Toksöz (1987), Chen and Schuster (1999), and Berkhout *et al.* (2001), but now includes an imaginary part. Figure 1 displays its real and imaginary part. Although the original scatterer was real-valued, its resolution function or migration image has a substantial imaginary part. This can be observed in Fig. 2, showing a vertical cross-section through the scatterer. Note that a point scatterer of the form $\mathrm{i}\,\delta(\mathbf{x} - \mathbf{x}_p)$ would lead to a resolution function with an imaginary part identical to the real part of the earlier one and a real part equal to minus the imaginary part of the earlier one, as the result is linear in the scatterer model.

We took the migration result and used it to generate new data. Demigration of the real part of the migration image, displayed in the left panel of Fig. 1, produced one frequency-domain data set. Demigration of the imaginary part of the migration image, shown in the right panel of Fig. 1, produced another complex-valued frequency-domain data set, which we multiplied by i. We then applied a Fourier transform to

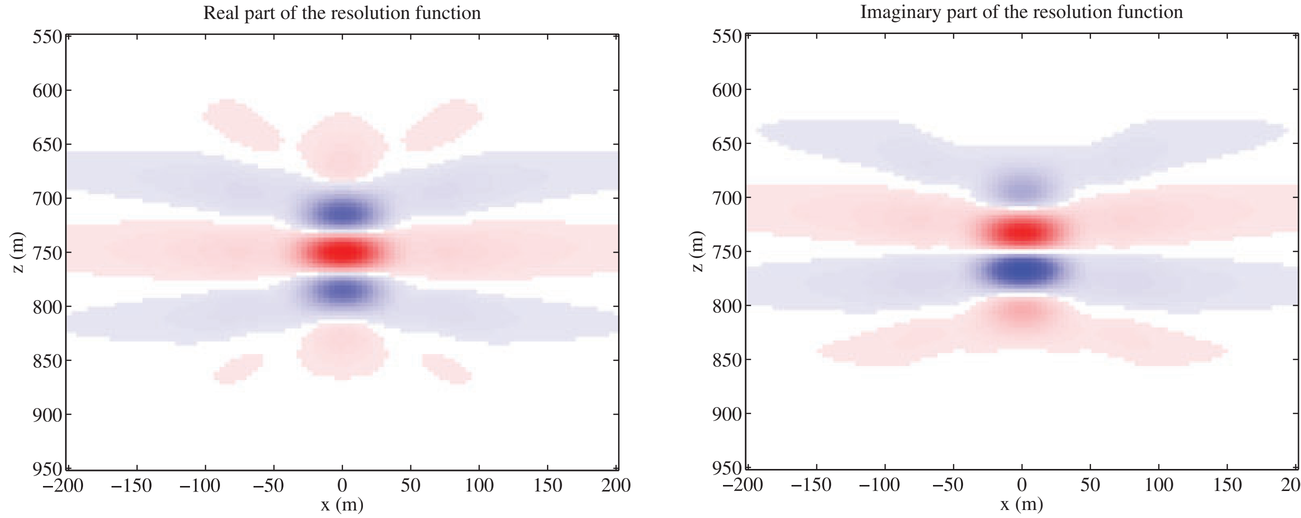

Figure 1 Real (left) and imaginary (right) part of the resolution function for a point scatterer at 750 m depth in a homogeneous background model. Colour scales are the same for both panels, with positive values in red and negative values in blue.

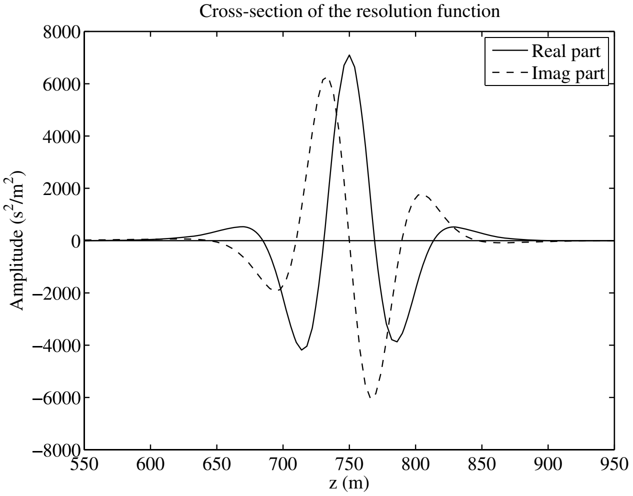

Figure 2 Real (drawn) and imaginary (dashed) part of the resolution function along the vertical cross-section going through the point scatterer at 750 m depth.

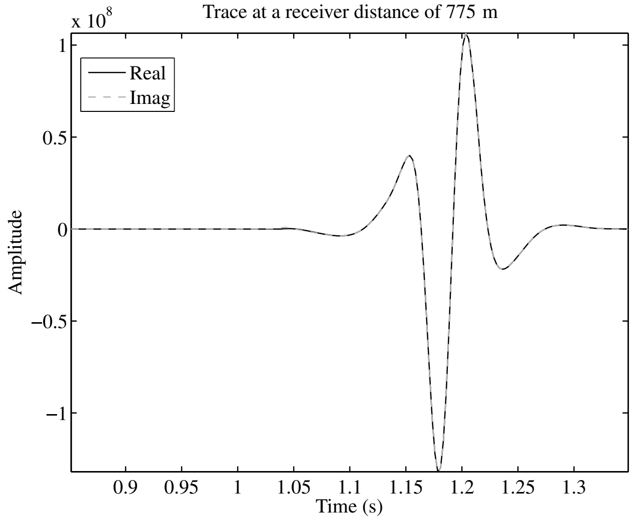

Figure 3 Data for a 2D scattering model. The black curve was obtained for a scattering model equal to the real part of the resolution function, the grey dashed line corresponds to i times its imaginary part. The curves are practically on top of each other.

obtain time-domain data. The resulting data sets turned out to be nearly identical. Figure 3 shows a single trace of each data set for a shot located at $x_s = -987.5$ m and a receiver at $x_r = 775$ m. We therefore have two different models that produce the same data. This suggests that, in the current example,

$$\mathsf{F}\left\{\mathrm{Re}\left[\sum_{\omega}\mathsf{F}^{\mathsf{H}}\mathsf{F}\right]\delta(\mathbf{x}-\mathbf{x}_p)\right\} \simeq \mathrm{i}\,\mathsf{F}\left\{\mathrm{Im}\left[\sum_{\omega}\mathsf{F}^{\mathsf{H}}\mathsf{F}\right]\delta(\mathbf{x}-\mathbf{x}_p)\right\}. \tag{5}$$

This states that a scattering model that equals the real part of the resolution function produces nearly the same data as a model that equals i times the imaginary part of the resolution function. Appendix A demonstrates that a similar approximate equality holds for a 1D, horizontally layered scattering model in a constant 3D background. The present numerical result suggests a generalization to a 2D scattering model in a constant 2D background. So far, we have not attempted to prove equation (5).

Next, we consider the reconstruction of the original scattering model given the seismic data for the specific acquisition and source signature. Because H is singular, we have to resort to its pseudo-inverse, also known as generalized or Moore-Penrose inverse, $\mathsf{H}^\dagger$, which can be computed from its singular-value decomposition $\mathsf{H} = \mathsf{V}\mathsf{D}\mathsf{V}^{\mathsf{H}}$. Here D is a diagonal matrix that contains the eigenvalues. Because H is Hermitian, the eigenvalues are real. Because H is the product of F and its conjugate transpose, these eigenvalues are non-negative. The columns of V contain the corresponding orthonormal eigenvectors. Therefore, $\mathsf{V}^{-1} = \mathsf{V}^{\mathsf{H}}$. The pseudo-inverse becomes $\mathsf{H}^\dagger = \mathsf{V}\mathsf{D}^\dagger\mathsf{V}^{\mathsf{H}}$, where $\mathsf{D}^\dagger$ contains the inverse for non-zero elements and has a zero otherwise. Because of the presence of numerical round-off errors, we assumed an eigenvalue to be zero if it was smaller than 10^{-14} times the largest eigenvalue. Figure 4 shows the eigenvalues of H, the elements of D, for the current example.

The 'best' reconstruction of the scatterer is given by $\mathbf{m}_1 = \mathsf{H}^\dagger\mathsf{H}\,\mathbf{m}$. Figure 5 displays the reconstruction $\mathbf{m}_1$ for a point scatterer with real-valued, unit amplitude located at

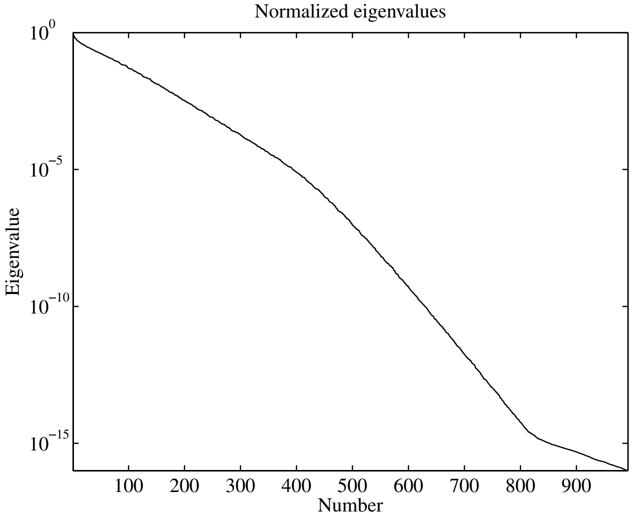

Figure 4 The eigenvalues of the Hessian, normalized by the largest eigenvalue. Values smaller than 10^{-16} are not shown.

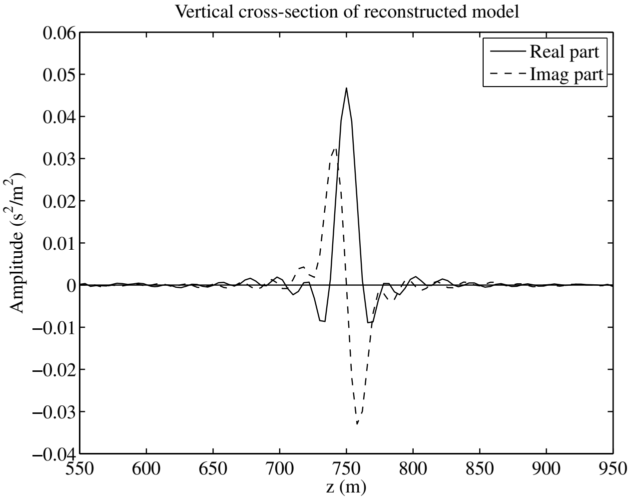

Figure 5 Real (drawn) and imaginary (dashed) part of a vertical cross-section through the reconstruction of the point scatterer at 750 m depth.

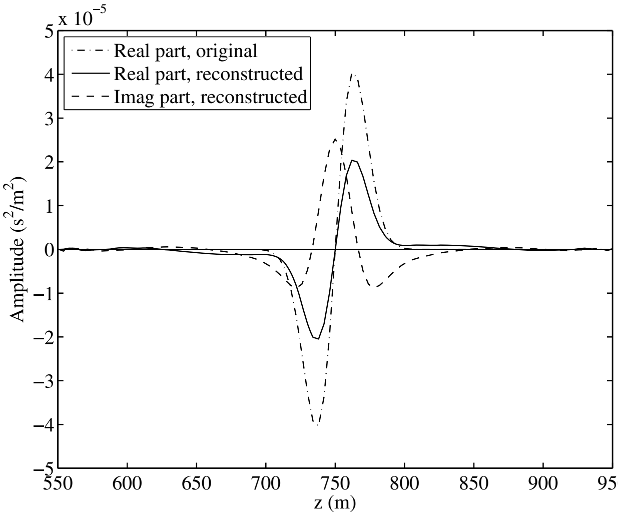

Figure 6 Real (drawn) and imaginary (dashed) part of a vertical cross-section through the reconstruction of an extended scatterer centred at 750 m depth. The dash-dotted line represents the original scatterer, which has a zero imaginary part.

$x_p = y_p = 0$ m and $z_p = 750$ m. Again, we observe a substantial contribution in the imaginary part. To convince ourselves that this is not a result of the limited bandwidth imposed by the Ricker wavelet, we repeated the exercise for an extended scatterer, the z-derivative of Gaussian:

$$m_g(x, z) = -\frac{\partial}{\partial z}\frac{1}{2\pi\sigma_g^2}\exp\left(-\frac{(x-x_p)^2+(z-z_p)^2}{2\sigma_g^2}\right).$$

We set $\sigma_g = 13.3$ m, at one tenth of the wavelength corresponding to the peak frequency of the wavelet. Figure 6 shows a vertical line through the original, purely real-valued scatterer and the real and imaginary part of its reconstruction. Again, the imaginary part has about the same amplitude as the real part.

The real and imaginary part of the resolution function are approximately related by a z-weighted Hilbert transform for 1D horizontally layered scattering models and also on the symmetry line through a localized scatterer. We discussed this in detail in Mulder and Hak (2009). We showed that two scattering models, related by a depth-weighted Hilbert transform, will produce approximately the same data. This implies that for the reconstruction problem, we can select any linear combination of those two models. Migration selects the one with the smallest norm, as does the pseudo-inverse of the Hessian.

Next, we will search for cases were the ambiguity can be fully or partially removed.

4 OTHER ACQUISITION GEOMETRIES

The ambiguity in the reconstruction of a scattering model shows up for a surface acquisition. We investigated if the same is true for other acquisition geometries. We start with a circle around a scattering object, continue with a cross-well example, and then consider diving waves in a velocity model that is linear in depth.

Circle

An acquisition geometry with source and receivers on a circle surrounding the scatterer provides optimal illumination. We placed 90 sources and 90 receivers on a circle with a radius of 750 m around the point scatterer, interleaved at regular angles. Figure 7 shows a vertical cross-section of the resolution function obtained with a 15-Hz Ricker wavelet for this acquisition. The cross-section cuts through the position of the scatterer. The resolution function has circular symmetry around this point for the chosen acquisition geometry. Its imaginary part is nearly invisible in the image. A similar section of the reconstructed model, obtained by using the pseudo-inverse of the Hessian, is displayed in Fig. 8. Clearly, the ambiguity does not show up in this ideal setting. Ribodetti *et al.* (2000) found a similar result.

The high degree of symmetry leaves no room for an antisymmetric imaginary part in this example. We therefore repeated

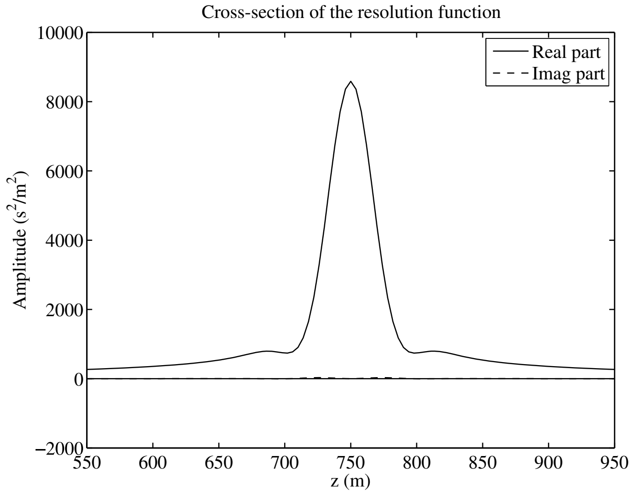

Figure 7 Real (drawn) and imaginary (dashed) part of the resolution function along a vertical cross-section through the point scatterer at 750 m depth for a circular acquisition geometry.

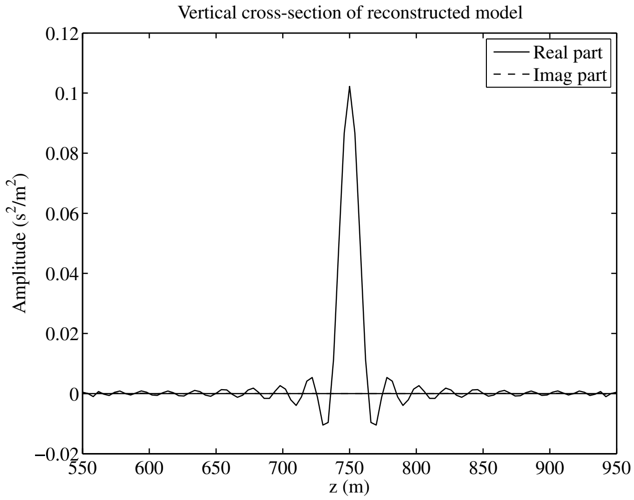

Figure 8 Real (drawn) and imaginary (dashed) part of the reconstructed model along a vertical cross-section through the point scatterer at 750 m depth for a circular acquisition geometry.

the computations for a shifted circle, centred at the same $x = 0$ m but with a shallower depth of $z = 550$ m. The real part of the resolution function is quite similar to the earlier case of a circular acquisition centred around the scatterer, but its imaginary part, displayed in Figs 9 and 10, is now non-zero. The reconstructed model, however, has a negligible imaginary part and is nearly identical to the earlier result shown in Fig. 8. Its horizontal cross-section, not shown either, has the same shape as the vertical cross-section.

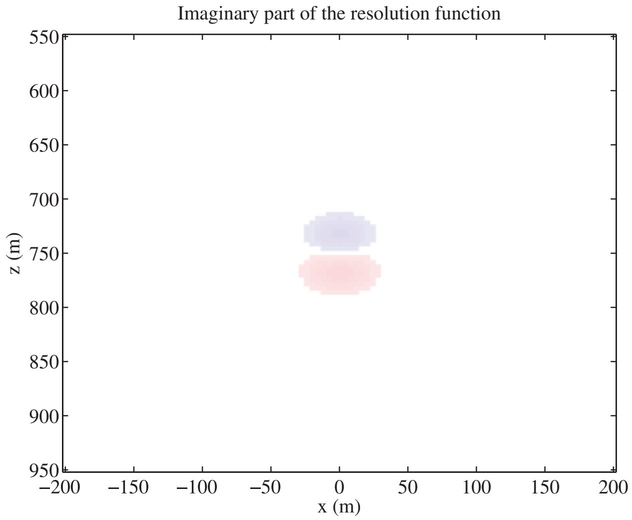

Figure 9 Imaginary part of the resolution function for a point scatterer at 750 m depth surrounded by sources and receivers on a shifted circle.

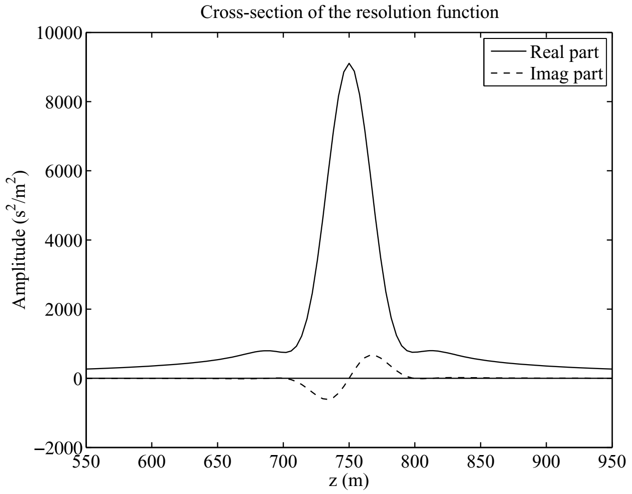

Figure 10 Real (drawn) and imaginary (dashed) part of the resolution function along a vertical cross-section through the point scatterer at 750 m depth for a shifted circular acquisition geometry.

Cross-well data

Placing sources and receivers all around a scatterer is difficult to realize in seismic exploration. A cross-well experiment comes close. We considered a highly symmetric acquisition geometry with two wells. Sources where placed at $x = -250$ m and receivers at $x = +250$ m, both at depths between 0–1500 m at a 25-m interval. The high degree of symmetry resulted in a negligible imaginary part, both for the resolution function and for the band-limited reconstruction of the point scatterer.

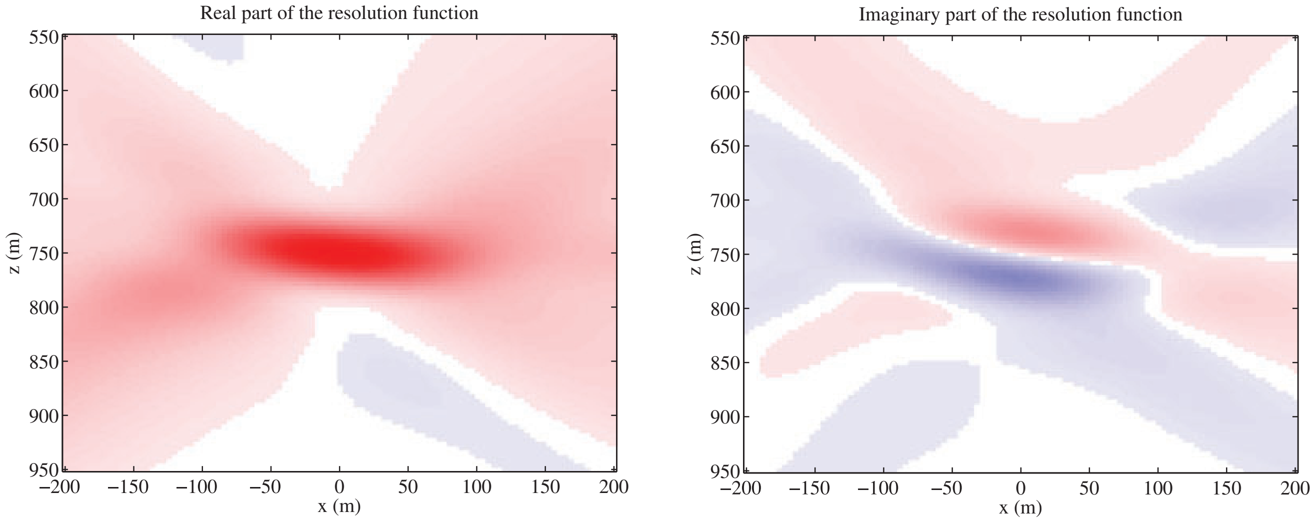

Figure 11 Real part (left) and imaginary part (right) of the resolution function for a point scatterer at 750 m depth for a cross-well configuration with sources and receivers in wells on either side of the scatterer. Colour scales are the same for both panels, with positive values in red and negative values in blue.

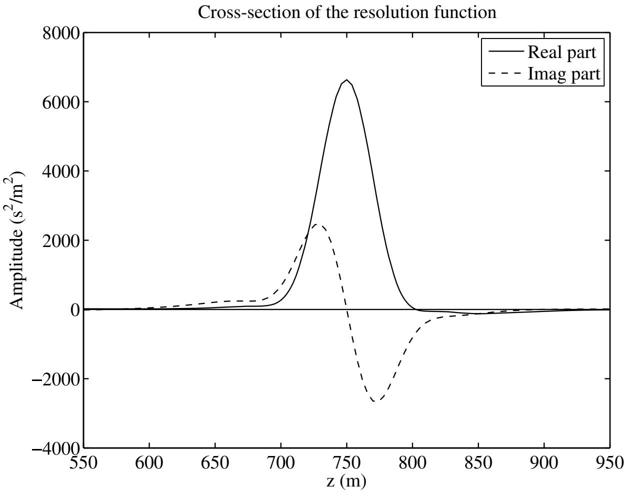

Figure 12 Real (drawn) and imaginary (dashed) part of the resolution function (top) along a vertical cross-section through the point scatterer at 750 m depth, for a cross-well acquisition geometry.

We also considered a less symmetric case by placing the sources at $x = -250$ m and the receivers at $x = +450$ m, with depths between 0–1000 m at a 25-m interval while keeping the point scatterer at $x = 0$ m and $z = 750$ m. Figures 11 and 12 display the real and imaginary part of the resolution function as well as a vertical section through the scattering point. Both the resolution function and the reconstructed parameter, shown in Fig. 13, have a non-negligible imaginary part, although its amplitude is considerably smaller than in the case of a surface acquisition. We conclude that a cross-well setting does not completely remove the ambiguity.

Diving waves

In the above, we have seen that a circular acquisition helps to remove the ambiguity, at least for the simple case considered, and that a cross-well setting does not do so completely, although the amplitude of the erroneous part is smaller than in the case of a surface acquisition. In the last case, we only have illumination from above. If, however, the velocity increases with depth as it typically does in an exploration setting, diving waves may improve the illumination, as they may illuminate the scatterer from below when travelling back to the surface. Figure 14 provides an illustration.

We considered a linear velocity model with $v(z) = v_0 + \alpha z$, setting $v_0 = 1.5$ km/s and $\alpha = 0.7$ 1/s. The Green function for the 2D case is (Kuvshinov and Mulder 2006)

$$G(\omega, \mathbf{x}_1, \mathbf{x}_2) = \frac{1}{2\pi}\left[Q_{\nu-1/2}(u)\right]^*,$$

with

$$u = 1 + \frac{(x_2 - x_1)^2 + (\hat{z}_2 - \hat{z}_1)^2}{2\hat{z}_2\hat{z}_1}.$$

$Q_{\nu-1/2}(u)$ is the Legendre function, $\nu = \mathrm{i}\sqrt{(\tilde{\omega}/\alpha)^2 - 1/4}$ and $\hat{z}_k = z_k + v_0/\alpha$ for $k = 1, 2$. Attenuation is included by letting $\tilde{\omega} = \omega[1 + (i - a)/(2Q)]$, with $a = (2/\pi)\log(f/f_r)$. We have

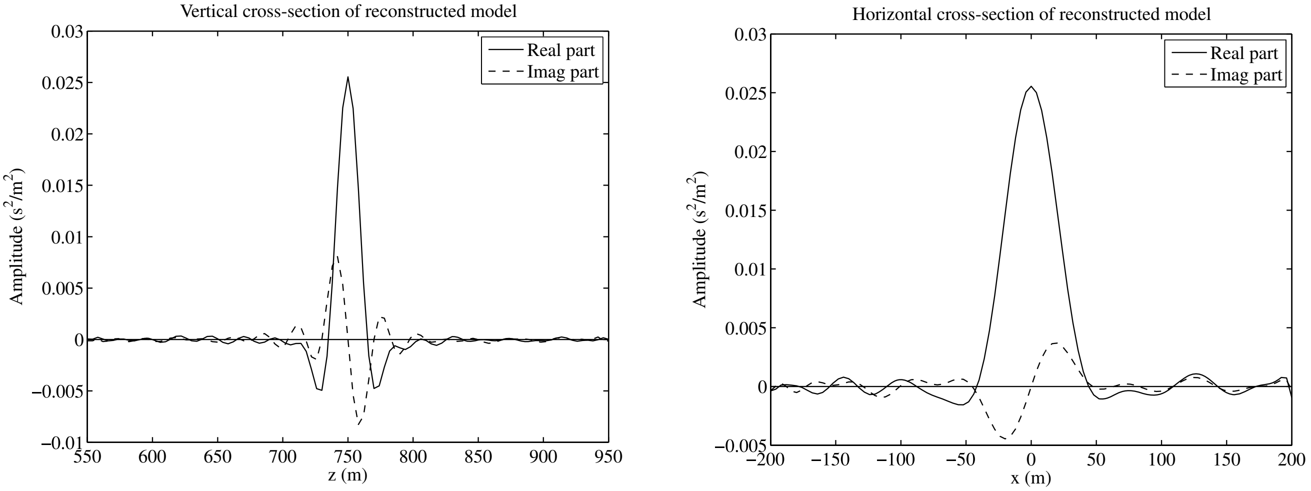

Figure 13 Real (drawn) and imaginary (dashed) part of the reconstructed scatterer along a vertical line (left) and horizontal line (right) through its original point scatterer position, for a cross-well acquisition geometry.

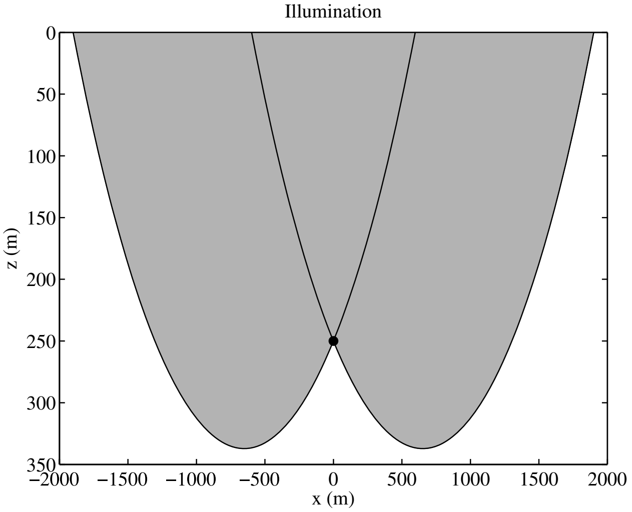

Figure 14 Illumination of a point scatterer in a velocity model that increases linearly with depth.

taken the complex conjugate because we adopted a Fourier convention opposite to the one used by Kuvshinov and Mulder (2006).

We chose the same acquisition and wavelet as in the first homogeneous example. Because diving waves do not reach that deep for this acquisition geometry (Mulder and Plessix 2008), we placed the point scatterer at a depth of 250 m. Figures 15–17 display the resolution function and the reconstruction of the point scatterer. There may be some numerical errors due to the truncation of the Hessian to the 200 × 200 m^2 subdomain. Nevertheless, it is apparent that we have a non-negligible imaginary part in the end result. Therefore, reconstruction of both velocity and attenuation perturbation will be difficult in this setting.

5 DISCUSSION AND CONCLUSIONS

We have extended the concept of the resolution function to the complex-valued case, meaning that not only impedance but also attenuation perturbations are taken into account. For the constant-density acoustic case with the Born approximation, we found that the resolution function cannot unambiguously distinguish between perturbations in velocity or in the quality factor that describes attenuation for an acquisition geometry with sources and receivers at the surface and a constant background model. This ambiguity was described in detail for horizontally layered scatterers in an earlier paper (Mulder and Hak 2009). Here, we observed a similar behaviour for a 2D scattering model: data generated in a constant background model for the resolution function of a point scatterer were nearly identical when either the real part of this resolution function was used as a scattering model or i times its imaginary part. As a consequence, simultaneous linearized inversion for velocity and attenuation perturbation is nearly impossible.

We considered alternative acquisition geometries that potentially could reduce or remove the ambiguity. Sources and receivers on a circle surrounding the scatterer led to an

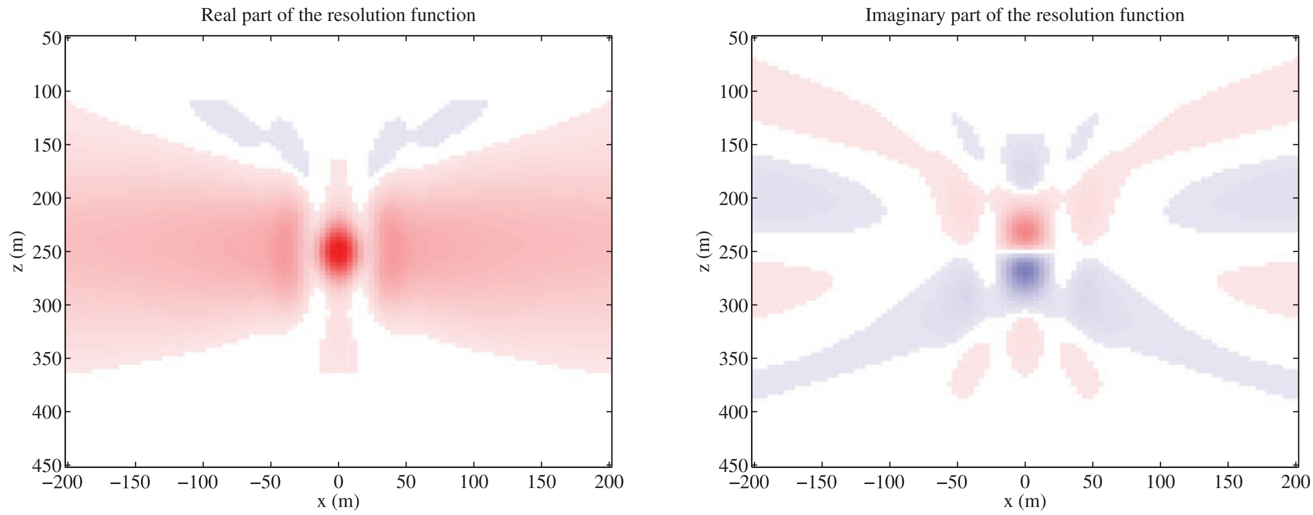

Figure 15 Real part (left) and imaginary part (right) of the resolution function for a point scatterer at 250 m depth in a linear velocity model. Colour scales are the same for both panels, with positive values in red and negative values in blue.

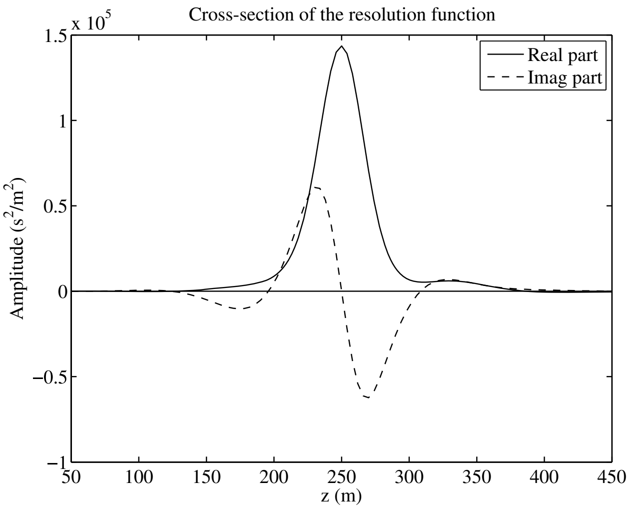

Figure 16 Real (drawn) and imaginary (dashed) part of the resolution function (top) along a vertical cross-section through the point scatterer at 750 m depth, in a linear background velocity model.

unambiguous result, apart from the usual limitations caused by the finite bandwidth of the acoustic measurements. A circular acquisition is natural in, for instance, medical application but for hydrocarbon exploration, a circular, buried acquisition is impractical and costly. We therefore examined a crosswell geometry as an alternative. Except in an exceptional case with high symmetry, the ambiguity reappears but is not as strong as in the surface case.

Diving waves in a model that has the velocity increasing linearly with depth will improve the illumination of a shallow target compared to down- and up-moving waves reflecting in a constant model. Nevertheless, this kind of illumination still provides a substantial attenuative component after migration for data that are based on a pure velocity perturbation. This leads to the conclusion that migration of seismic data to map both velocity and attenuation perturbations is prone to large errors.

The question remains if non-linear inversion of seismic data will improve the situation and allow for the unambiguous determination of subsurface attenuation parameters. The work of Hicks and Pratt (2001) suggested that this may very well be the case, possibly with first carrying out the velocity updates of the model and then performing the attenuation updates (Hicks and Pratt 2001; Rao and Wang 2008). Another question is how the incorporation of the causality in the scatterer, which we ignored here for simplicity, will affect the linear inversion. Including causality will lead to frequency-dependent behaviour that may help to reduce or even remove the ambiguity when a sufficiently large range of frequencies is used.

ACKNOWLEDGEMENTS

This work is part of the research programme of the Stichting voor Fundamenteel Onderzoek der Materie (FOM), financially supported by the Nederlandse Organisatie voor

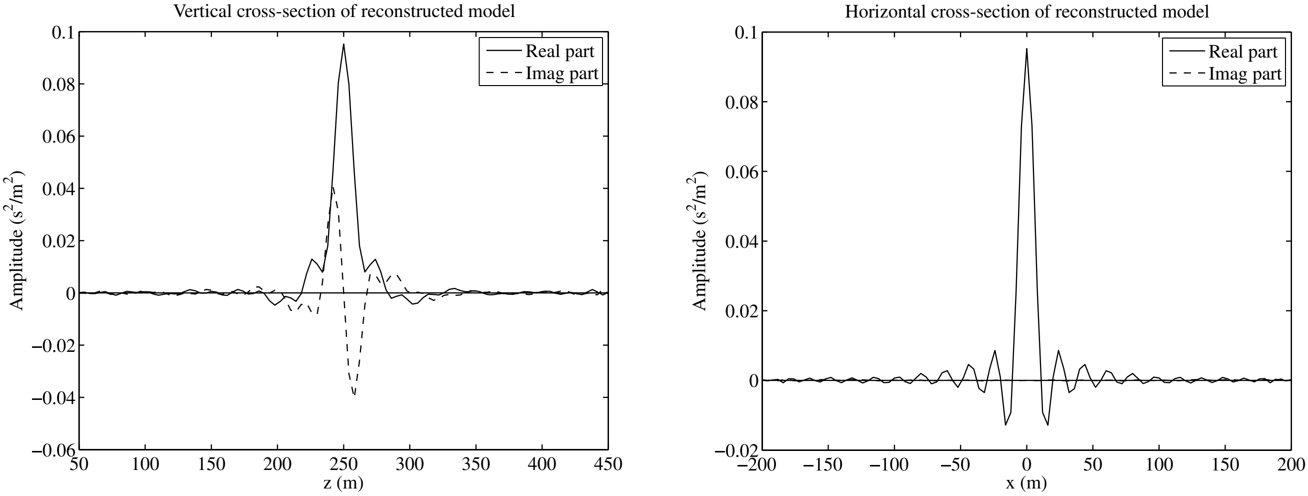

Figure 17 Real (drawn) and imaginary (dashed) part of the reconstructed scatterer along a vertical line (left) and horizontal line (right) through the original point scatterer position, in a linear background velocity model.

Wetenschappelijk Onderzoek (NWO) and the Stichting Shell Research.

REFERENCES

Aki K. and Richards P.G. 1980. *Quantitative Seismology: Theory and Methods, Volume I*. W.H. Freeman and Company. ISBN 0716710587.

Barnes C., Charara M. and Tsuchiya T. 2008. Feasibility study for an anisotropic full waveform inversion of cross-well seismic data. *Geophysical Prospecting* **56**, 897–906.

Berkhout A.J., Ongkiehong L., Volker A.W.F. and Blacquière G. 2001. Comprehensive assessment of seismic acquisition geometries by focal beams – Part I: Theoretical considerations. *Geophysics* **66**, 911–917.

Beylkin G. and Burridge R. 1990. Linearized inverse scattering problems in acoustics and elasticity. *Wave Motion* **12**, 15–52.

Bleistein N., Cohen J.K. and Stockwell J.W. 2000. *Mathematics of Multidimensional Seismic Imaging, Migration, and Inversion*. Springer–Verlag. ISBN 0387950613.

Causse E., Mittet R. and Ursin B. 1999. Preconditioning of full-waveform inversion in viscoacoustic media. *Geophysics* **64**, 130–145.

Chavent G. and Plessix R.E. 1999. An optimal true-amplitude least-squares prestack depth-migration operator. *Geophysics* **64**, 508–515.

Chen J. and Schuster G.T. 1999. Resolution limits of migrated images. *Geophysics* **64**, 1046–1053.

Crase E., Pica A., Noble M., McDonald J. and Tarantola A. 1990. Robust elastic nonlinear waveform inversion: Application to real data. *Geophysics* **55**, 527–538.

Crase E., Wideman C., Noble M. and Tarantola A. 1992. Nonlinear elastic waveform inversion of land seismic reflection data. *Journal of Geophysical Research* **97**, 4685–4703.

Devaney A.J. 1984. Geophysical diffraction tomography. *IEEE Transactions on Geoscience and Remote Sensing* **GE-22**, 3–13.

Docherty P. 1991. A brief comparison of some Kirchhoff integral formulas for migration and inversion. *Geophysics* **56**, 1164–1169.

Gélis C., Virieux J. and Grandjean G. 2007. Two-dimensional elastic full waveform inversion using Born and Rytov formulations in the frequency domain. *Geophysical Journal International* **168**, 605–633.

Gjøystdal H., Iversen E., Laurain R., Lecomte I., Vinje V. and Åstebøl K. 2002. Review of ray theory applications in modelling and imaging of seismic data. *Studia Geophysica et Geodaetica* **46**, 113–164.

Gray S. 1997. True-amplitude migration: a comparison of three approaches. *Geophysics* **62**, 929–936.

Guitton A. 2004. Amplitude and kinematic corrections of migrated images for nonunitary imaging operators. *Geophysics* **69**, 1017–1024.

Hak B. and Mulder W.A. 2008a. Preconditioning for linearised inversion of attenuation and velocity perturbations. 70th EAGE meeting, Rome, Italy, Extended Abstracts, H002.

Hak B. and Mulder W.A. 2008b. Preconditioning for linearized inversion of attenuation and velocity perturbations. 78th SEG meeting, Las Vegas, Nevada, USA, Expanded Abstracts, 2036–2040.

Hicks G.J. and Pratt R.G. 2001. Reflection waveform inversion using local descent methods: Estimating attenuation and velocity over a gas-sand deposit. *Geophysics* **66**, 598–612.

Innanen K.A. and Weglein A.B. 2007. On the construction of an absorptive-dispersive medium model via direct linear inversion of reflected seismic primaries. *Inverse Problems* **23**, 2289–2310.

Jin S., Madariaga R., Virieux J. and Lambaré G. 1992. Two-dimensional asymptotic iterative elastic inversion. *Geophysical Journal International* **108**, 575–588.

Kennett B.L.N. and Sambridge M. 1998. Inversion for multiple parameter classes. *Geophysical Journal International* **135**, 304–306.

Kennett B.L.N., Sambridge M.S. and Williamson P.R. 1988. Subspace methods for large inverse problems with multiple parameter classes. *Geophysical Journal International* **94**, 237–247.

Kuvshinov B.N. and Mulder W.A. 2006. The exact solution of the time-harmonic wave equation for a linear velocity profile. *Geophysical Journal International* **167**, 659–662.

Lailly P. 1983. The seismic inverse problem as a sequence of before stack migration. In: *Proceedings of the Conference on Inverse Scattering: Theory and Applications* (eds J.B. Bednar, R. Redner, E. Robinson and A. Weglein), pp. 206–220. SIAM, Philadelphia. ISBN 0898711908.

Lambaré G., Virieux J., Madariaga R. and Jin S. 1992. Iterative asymptotic inversion in the acoustic approximation. *Geophysics* **57**, 1138–1154.

Mora P. 1987. Nonlinear two-dimensional elastic inversion of multioffset seismic data. *Geophysics* **52**, 1211–1228.

Mora P. 1988. Elastic wave-field inversion of reflection and transmission data. *Geophysics* **53**, 750–759.

Mora P. 1989. Inversion = migration + tomography. *Geophysics* **54**, 1575–1586.

Mulder W.A. and Hak B. 2009. An ambiguity in attenuation scattering imaging. *Geophysical Journal International* **178**, 1614–1624.

Mulder W.A. and Plessix R.E. 2004. A comparison between one-way and two-way wave-equation migration. *Geophysics* **69**, 1491–1504.

Mulder W.A. and Plessix R.E. 2008. Exploring some issues in acoustic full waveform inversion. *Geophysical Prospecting* **56**, 827–841.

Nemeth T., Wu C. and Schuster G.T. 1999. Least-squares migration of incomplete reflection data. *Geophysics* **64**, 208–221.

Operto S., Ravaut C., Improta L., Virieux J., Herrero A. and Dell'Aversana P. 2004. Quantitative imaging of complex structures from dense wide-aperture seismic data by multi-scale traveltime and waveform inversions: a case study. *Geophysical Prospecting* **52**, 625–651.

Østmo S., Mulder W.A. and Plessix R.E. 2002. Finite-difference iterative migration by linearized waveform inversion in the frequency domain. 72nd SEG meeting, Salt Lake City, Utah, USA, Expanded Abstracts, 1384–1387.

Plessix R.E. and Mulder W.A. 2004. Frequency-domain finite-difference amplitude-preserving migration. *Geophysical Journal International* **157**, 975–987.

Pratt R.G. 1999. Seismic waveform inversion in the frequency domain, Part 1: Theory and verification in a physical scale model. *Geophysics* **64**, 888–901.

Pratt R.G., Shin C.S. and Hicks G.J. 1998. Gauss-Newton and full Newton methods in frequency-space seismic waveform inversion. *Geophysical Journal International* **133**, 341–362.

Rao Y. and Wang Y.H. 2008. The strategies for attenuation inversion with waveform tomography. 70th EAGE meeting, Rome, Italy, Extended Abstracts, H006.

Ribodetti A., Operto S., Virieux J., Lambaré G., Valéro H. and Gibert D. 2000. Asymptotic viscoacoustic diffraction tomography of ultrasonic laboratory data: a tool for rock properties analysis. *Geophysical Journal International* **140**, 324–340.

Ribodetti A. and Virieux J. 1998. Asymptotic theory for imaging the attenuation factor Q. *Geophysics* **63**, 1767–1778.

Ribodetti A., Virieux J. and Durand S. 1995. Asymptotic theory for viscoacoustic seismic imaging. 65th SEG meeting, Houston, Texas, USA, Expanded Abstracts, 631–634.

Rickett J.E. 2003. Illumination-based normalization for wave-equation depth migration. *Geophysics* **68**, 1371–1379.

Royle G.T. and Singh S.C. 2008. Viscoelastic modeling and full waveform inversion in attenuating media. 70th EAGE meeting, Rome, Italy, Workshop WO11, 121–125.

Shin C., Jang S. and Min D.J. 2001. Improved amplitude preservation for prestack depth migration by inverse scattering theory. *Geophysical Prospecting* **49**, 592–606.

Shipp R.M. and Singh S.C. 2002. Two-dimensional full wavefield inversion of wide-aperture marine seismic streamer data. *Geophysical Journal International* **151**, 325–344.

Symes W.W. 2008. Approximate linearized inversion by optimal scaling of prestack depth migration. *Geophysics* **73**, R23–R35.

Tarantola A. 1984. Inversion of seismic reflection data in the acoustic approximation. *Geophysics* **49**, 1259–1266.

Tarantola A. 1986. A strategy for nonlinear elastic inversion of seismic reflection data. *Geophysics* **51**, 1893–1903.

ten Kroode A.P.E., Smit D.J. and Verdel A.R. 1998. A microlocal analysis of migration. *Wave Motion* **28**, 149–172.

Toxopeus G., Petersen S., Thorbecke J. and Wapenaar K. 2004. Simulating high resolution inversion: decomposing the resolution function. 74th SEG meeting, Denver, Colorado, USA, Expanded Abstracts, 1798–1801.

Toxopeus G., Thorbecke J., Wapenaar K., Petersen S., Slob E. and Fokkema J. 2008. Simulating migrated and inverted seismic data by filtering a geologic model. *Geophysics* **73**, T1–T10.

van Houten E.E.W., Paulsen K.D., Miga M.I., Kennedy F.E. and Weaver J.B. 1999. An overlapping subzone technique for MR-based elastic property reconstruction. *Magnetic Resonance in Medicine* **42**, 779–786.

Vasheghani F. and Lines L.R. 2009. Viscosity and Q in heavy-oil reservoir characterization. *The Leading Edge* **28**, 856–860.

von Seggern D. 1991. Spatial resolution of acoustic imaging with the Born approximation. *Geophysics* **56**, 1185–1202.

Wapenaar C.P.A. 1997. 3-D migration of cross-spread data: resolution and amplitude aspects. *Geophysics* **62**, 1220–1225.

Wu R.S. and Toksöz M.N. 1987. Diffraction tomography and multisource holography applied to seismic imaging. *Geophysics* **52**, 11–25.

APPENDIX A: DEMIGRATION FOR A 1D SCATTERING MODEL

Equation (5) states that demigration of the real part of the migration image obtained from data for a real-valued point scatterer in a 2D homogeneous background model produces complex-valued frequency-domain data that are nearly the same as those resulting from demigration of i times the imaginary part of that migration image. Here, we will demonstrate that a similar statement holds for a 1D layered scattering model $m(z)$ in a 3D homogeneous background. For this case, we showed earlier (Mulder and Hak 2009) that we obtain approximately the same data for a model and its scaled, depth-weighted Hilbert transform. These data obey

$$\mathsf{F}\mu \simeq -\mathrm{i}\mathsf{F}\breve{\mu}, \tag{A1}$$

with $\mu = m(z)/z$. The abbreviation $\breve{\mu} = \mathcal{H}_z[\mu]$ denotes the Hilbert transform of μ in depth. If $m(z)$ is localized, so nonzero for only a small range of z and z is not too small, the $1/z$ scaling can be ignored. We also showed that migration produces $\mu_0(z)$ with the property that

$$\mu_0 \simeq \tfrac{1}{2}(\mu - \mathrm{i}\breve{\mu}), \tag{A2}$$

if suitable migration weights are used. If the original μ has a zero imaginary part, which we emphasize by setting $\mu = \mu_r$, then $\mathrm{Re}\,\mu_0 \simeq \frac{1}{2}\mu_r$ and $\mathrm{Im}\,\mu_0 \simeq -\frac{1}{2}\breve{\mu}_r$. We can select the real part of μ_0 as a new scattering model to produce data $\mathsf{F}\{\mathrm{Re}\,\mu_0\}$. Combining equations (A1) and (A2), we obtain

$$\mathsf{F}\{\mathrm{Re}\,\mu_0\} \simeq \tfrac{1}{2}\mathsf{F}\mu_r \simeq -\tfrac{1}{2}\mathrm{i}\,\mathsf{F}\breve{\mu}_r \simeq \mathrm{i}\,\mathsf{F}\{\mathrm{Im}\,\mu_0\}\,.$$

This agrees with the more general expression in equation (5), found numerically for a point scatterer in a 2D homogeneous background.